Unique Temperature Trend Pattern Associated with Internally Driven Global Cooling and Arctic Warming during 1980-2022

Aodhan J. Sweeney[1], Qiang Fu[1], Stephen Po-Chedley[2], Hailong Wang[3], Muyin Wang[4,5]

[1]University of Washington, Department of Atmospheric Sciences
[2]Program for Climate Model Diagnosis and Intercomparison, Lawrence Livermore National Laboratory, Livermore, CA, USA
[3]Atmospheric, Climate, and Earth Sciences Division, PNNL
[4]University of Washington, Cooperative Institute for Climate, Ocean, and Ecosystem Studies
[5]Pacific Marine Environmental Laboratory, Oceanic and Atmospheric Research, NOAA

Corresponding authors: Aodhan Sweeney (aodhan@uw.edu) and Qiang Fu (qfu@uw.edu)

Key Points:

- Internal variability has enhanced Arctic warming but suppressed global warming over 1980-2022.
- This manifestation of internal variability is rare in model simulations but has a robust global surface air temperature (SAT) trend pattern.
- This internal SAT pattern features warming in the Barents and Kara Sea and cooling of the tropical Eastern Pacific and Southern Ocean.

Abstract

Diagnosing the role of internal variability over recent decades is critically important for both model validation and projections of future warming. Recent research suggests that for 1980-2022 internal variability manifested as Global Cooling and Arctic Warming (i-GCAW), leading to enhanced Arctic Amplification (AA) and suppressed global warming over this period. Here we show that the observationally derived i-GCAW is rare in CMIP6 large ensembles, but simulations that do produce similar i-GCAW exhibit a unique and robust internally driven global surface air temperature (SAT) trend pattern. This unique pattern of SAT change features enhanced warming in Barents and Kara Sea and cooling in the tropical Eastern Pacific and Southern Ocean. Given that these features are imprinted in the observed record over recent decades, this work suggests that internal variability makes a crucial contribution to the discrepancy between model-simulated forced SAT trend pattern and observations.

Plain Language Summary

When comparing model simulations of Earth's recent warming to real-world observations, differences may arise from several factors. Two important factors are the model errors in the simulated response to increased greenhouse gases, and natural fluctuations within the climate system that produced discrepancies between observations and models. Thus, quantifying the role of these natural fluctuations are important for the assessment of model-observation differences. Previous studies have shown that natural climate variability has depressed global warming and enhanced Arctic warming. By compositing simulations in which natural variability warms the Arctic but has an overall cooling effect globally, we find that the majority of these model simulations also produce enhanced warming in the Barents and Kara Seas and cooling in the Tropical Pacific and Southern Ocean due to natural variability. Since these are the exact features imprinted on observed surface temperature changes over 1980-2022, our work suggests natural variability is an important component of several noteworthy differences between models and observations.

1 Introduction

Global surface air temperatures (SAT) since 1980 have experienced significant warming due to increased greenhouse gas concentrations and reduced aerosols (IPCC, 2021). Yet, the pattern of the observed warming has larger spatial variability than the warming simulated by climate models (e.g., Hansen et al., 2010). One of the most prominent features of both observed and simulated warming is Arctic Amplification (AA): the increased rate of Arctic warming compared to global mean surface temperature change (Manabe and Weatherald, 1975). From 1980 to 2022 observed SAT in the Arctic (defined as the region poleward of 70°N) warmed about four times faster than the global mean, leading to an AA of about 4.0. Although models simulate greater Arctic warming relative to the global mean, the observed values of AA over 1980 to 2022 are larger than AAs from 94% of historical simulations from large ensembles in the Coupled Model Intercomparison Project Phase 6 (CMIP6) (Hahn et al., 2021; Ye and Messori, 2021; Rantanen et al., 2022; Chylek et al., 2022; Chylek et al., 2023; Sweeney et el., 2023). The discrepancy between the model predicted AA and that observed from 1980-2022 may be due to a

model bias in the forced response of the Arctic and/or global climate, leading to concerns regarding model fidelity (Rosenblum and Eiseman, 2017; Chylek et al., 2022). Another potential cause of this discrepancy is a rare configuration of internal climate variability in the last four decades (Deser et al., 2012a; Deser et al., 2012b; Kay et al., 2011; Chylek et al., 2023; Feng et al., 2021). Key to reconciling this model-observation discrepancy is separating the forced response from internal variability (e.g., Lehner and Deser, 2023).

Various methodologies have been proposed to partition the forced and internal components of climate change (e.g., Foster and Rahmstorf, 2011; Wallace et al., 2012; Deser et al., 2014; Santer et al., 2014; Dai et al., 2015; Barnes et al., 2019; Räisänen, 2021; Gordon et al., 2021; Po-Chedley et al., 2022; Rader et al., 2022). Pattern recognition algorithms have shown promise with this task (Wills et al., 2020), because the SAT response to external forcing is more spatially uniform than the more complex patterns associated with internal variability. The patterns of the forced response and internal variability can be differentiated in large ensembles, which contain many simulations of the Earth's climate with varying initial conditions and then produce unique manifestations of the internal variability (and thus unique patterns of warming) (Kay et al., 2015; Deser et al., 2020). Large ensembles therefore provide a useful training dataset for pattern recognition algorithms designed to distinguish between the forced and unforced climate response. Recently, Sweeney et al. (2023) (referred to herein as S2023) showed that the pattern recognition algorithms based on machine learning can help partition the role of internal variability and the forced response to better understand the model-observation discrepancy in AA from 1980-2022. Their results indicate that internal variability has enhanced AA for 1980-2022 by 38%. After removing the contribution of internal variability from the observations, they can reconcile differences between simulated and observed AA.

The identified manifestation of internal variability that creates the exceptionally high value of observed AA features internally driven global-cooling and Arctic-warming (referred to hereafter as i-GCAW). When this i-GCAW pattern is imprinted onto the Earth's warming due to external forcing, the effect is to enhance the rate of Arctic warming while damping the global mean warming trend during 1980-2022. A number of studies have suggested that internal variability has warmed the Arctic (e.g., Chen and Dai, 2024) and cooled the globe in the last few decades, evidenced by rapid sea ice concentration decline (e.g., Ding et al., 2019) and a lack of warming (or even cooling) in the tropical Eastern Pacific and Southern Ocean (e.g., Kosaka and Xie, 2013; Po-Chedley et al., 2021; Zhang et al., 2019; Feng et al., 2021). These studies reinforce the result from S2023 that internal variability produced global-cooling and Arctic-warming during 1980-2022.

This study aims to investigate model simulations that have an imprint of i-GCAW. These simulations can provide insight into the global internally driven trend pattern since 1980. It thus has value for understanding model-observation discrepancies and may help constrain uncertainty in future patterns of SAT change (Lehner and Deser, 2023). Here we first show that the observationally derived i-GCAW in S2023 occurs rarely in the ensemble members from various GCMs and confirm that the machine learning algorithms developed in S2023 have minimal biases when applied to this subset of rare ensemble members. We then show that the ensemble members featuring similar i-GCAW to observationally derived values share a preferred internally driven global SAT trend pattern, including warming in the Barents and Kara Sea and cooling in the tropical Eastern Pacific and Southern Ocean. We further examine the pattern of differences between the observed SAT trend pattern and the forced warming pattern derived

from the CMIP6 multi-model mean scaled by observationally derived forced global-mean SAT trend in S2023. The difference trend pattern – which represents an estimate of the impact of internal variability on the pattern of satellite era SAT trends – also shows warming in the Kara Sea and cooling of the tropical Eastern Pacific and Southern Ocean. Both approaches indicate a common imprint of internal variability on the pattern of surface warming during recent decades. Finally, we examine the evolution of AA over the ensuing 20 years in the ensemble members that exhibit i-GCAW over a 43-year period (matching the length of the observational record from 1980-2022). These simulations suggest a decrease of the mean AA from 4.2 to 3.4, supporting the claim in S2023 that the exceptional AA over 1980 to present will not persist into the future.

2 Data

Data used here is the same as from S2023. The model simulations come from large ensembles included in CMIP6 using 10 different models that contain 10 to 50 ensemble members. Aside from the CMIP6 models, we also include the CESM2 large ensemble with updated biomass burning aerosol emissions (Rodgers et al., 2021; Fasullo et al., 2022). Using these 11 large ensembles, SAT trend maps are calculated using 43-year periods separated by five years spanning 1850-2047 (i.e., 1850-1892, 1855-1897, …, 1980-2022, …, 2005-2047). Historical simulations for the large ensembles end in 2014. For those models where more than 10 ensemble members have data through 2047 using the Shared Socioeconomic Pathways 3 or 5 (SSP3-7.00 or SSP5-8.5), the simulations are extended (using SSP5-8.5 when both are available) (O'Neill et al., 2016). Of the 11 large ensembles used, 7 have extensions past the 2014 period, while 4 end in 2014 (see Table S1 for information regarding the large ensembles).

We use 43-year trend periods to match the length of the observational SAT record from 1980-2022. Observational SAT trends shown here are the average of four datasets, including the Met Office Hadley Centre/Climate Research Unit's global surface temperature dataset version 5, Berkeley Earth Land/Ocean Temperature Record, GISS Surface Temperature Analysis version 4, and the NOAA Merged Land Ocean Global Surface Temperature Analysis version 5 (Morice et al., 2021; Rhode and Hausfather, 2020; Lenssen et al., 2019; Zhang et al., 2019). All SAT trend maps are regridded to a common 2.5°x2.5° latitude-by-longitude grid.

3 Internally Generated Global-Cooling and Arctic-Warming

Quantifying the internal component of recent SAT trends remains a crucial problem in climate science (Schlesinger and Ramankutty, 1994; Kosaka and Xie, 2013; Wanatabe et al., 2021; Wills et al., 2022). In this section, we show that a robust pattern of internal variability can be obtained by compositing model simulations with i-GCAW similar to observational derived values. As noted earlier, S2023 estimated that between 1980-2022, internal variability reduced observed global warming by 0.024 K/dec and enhanced Arctic warming by 0.145 K/dec. Across all 43-year SAT trends from the large ensembles between 1850-2047, the standard deviation of internally generated SAT trends over the globe and in the Arctic are 0.025 K/dec and 0.157 K/dec, respectively. Thus, when viewed individually, the observationally inferred estimates of internal variability are about one standard deviation from the mean, and thus not rare.

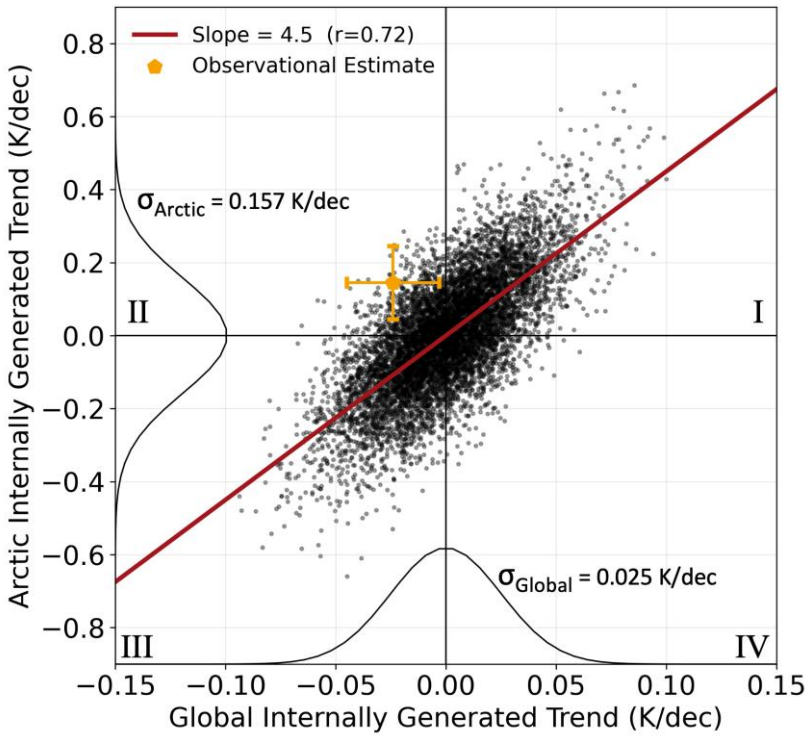

Figure 1: Arctic versus global internal trends from all large ensembles between 1850-2047. Each grey circle represents an internal trend from one ensemble member over one 43-year period. Thin black lines show the normalized probability density functions of all global and Arctic internal trends with the corresponding standard deviations provided. The orange pentagon shows the observationally derived internal trends for 1980-2022 with one-standard deviation error bars from S2023. The red line shows the linear regression of the Arctic internal trend onto that of the global internal trend, which has a slope of 4.5 and a correlation coefficient of 0.72. Roman numerals denote the quadrant number.

Given that internal variability both enhanced Arctic warming and depressed global warming, it is useful to examine the frequency of these events concurrently. Figure 1 shows the Arctic versus global mean internal trends for 43 years from all large ensembles over 1850-2047, indicating that Arctic and global internal trends are positively correlated in model simulations (r=0.72). While many studies have examined the coupling between global and Arctic temperature as a response to forced climate change, internal variability is also important to the coupling of global and Arctic temperature (Screen and Deser, 2019). The thick red line in Fig. 1 shows that the linear fit of Arctic to global internal trends has a slope of 4.5, meaning that an internally driven change in global SAT is typically amplified by a factor of 4.5 in the Arctic. This is analogous to Arctic Amplification but operating through multidecadal internal variability alone. 74% of all simulated 43-year trends are confined to quadrants I and III (top-right and bottom-left) in Fig. 1, where Arctic and global internal variability have the same sign. Only 26% of simulations exist in quadrants II and IV (top-left and bottom-right), where the Arctic and global internal trends have opposing signs. The observationally inferred trends of internal variability from S2023 sits in quadrant II (top-left). Quadrant II is a sparsely populated region, and the observational estimate is near the edge of the distribution suggesting that Earth experienced a rare configuration of internal variability over 1980-2022.

To gain confidence in the estimate from S2023 shown in Fig. 1, we deployed the previously trained algorithm used in S2023 to the subset of simulations which are in quadrant II and occur during 1980-2022. The resulting estimates of the internally driven component of the Arctic and global SAT trends only exhibit a small bias relative to their actual internal variability component. Note that the algorithm in S2023 was trained on cases from all quadrants. With this small bias, the inferred forced AA is very similar to results of S2023. For example, after accounting for this bias the inferred forced AA is 3.21, compared to the stated value of 3.03 in S2023. This indicates that the algorithm used in S2023 to estimate the role of global and Arctic internal variability can do so accurately in model simulations, even when those simulations occur with rare configurations of internal variability, including the observed manifestation of i-GCAW. This provides confidence that the estimated effects of internal variability are accurate.

The observationally inferred estimate from S2023 suggests that from 1980-2022 the Earth experienced i-GCAW. However, it does not provide information on the accompanying spatial pattern of the SAT trends. To investigate the SAT trend pattern associated with i-GCAW, we select 43-year trends in quadrant II with internally generated global cooling and Arctic warming magnitudes larger than $\sigma_{Global}/2$ and $\sigma_{Arctic}/2$, respectively (Fig. 1). We note that this threshold of i-GCAW is less than the observational estimate in Fig. 1 but is a lower limit. It is also chosen to make sure there is a sufficient number of samples in the subset. This subset contains 136 samples out of the original 8470 points in Fig. 1. These i-GCAW cases are thus a rare configuration of internal variability. These selected simulations show no obvious propensity for onset between 1850-2047, nor are these cases limited to a small subset of climate models (see Figure S1 and Table S1). Figure 2 shows the global internal SAT trend pattern averaged over the 136 i-GCAW cases. We repeated this calculation to produce average trend maps for quadrant I (internal Global Warming and Arctic Warming; i-GWAW), quadrant III (internal Global Cooling and Arctic Cooling; i-GCAC), and quadrant IV (internal Global Warming Arctic Cooling; i-GWAC), which are provided in Figure S2.

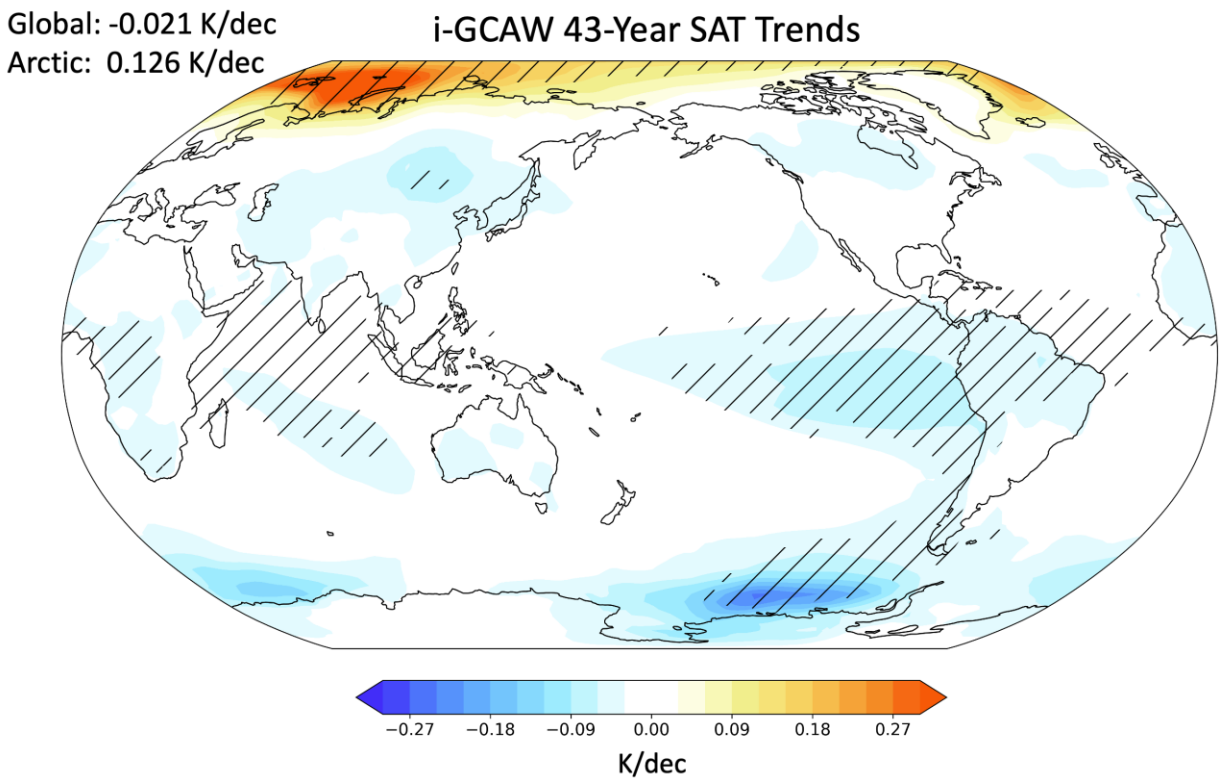

Figure 2: The 43-year SAT trend pattern due to internal variability averaged over 136 cases which have internally driven global cooling and Arctic warming (i-GCAW) magnitudes larger than $\sigma_{Global}/2$ and $\sigma_{Arctic}/2$ (see Fig. 1), respectively. Hatching represents the regions where over 80% of the cases agree on sign. The domain averaged Arctic and global mean temperature trends are provided on the top left.

The global trend pattern shown in Fig. 2 is derived entirely from model simulated internal variability based on simulations exhibiting internally generated global cooling and Arctic warming. The results suggest that i-GCAW has a preferred internal SAT trend pattern, which is unique compared to other configurations of internal variability shown in Fig. S2. Notable warming is featured in the Barents and Kara Sea relative to other locations in the Arctic, while cooling is evident throughout the tropical Eastern Pacific in addition to continental cooling in northern South America, central Africa, and parts of central Asia. A region of strong cooling is also located in the Amundsen Sea, linking tropical cooling of the Eastern Pacific into the Southern Ocean (Ding and Steig, 2013; Hwang et al., 2017; Stuecker et al., 2017; Dong et al., 2022). Interestingly, many of these features are sufficiently strong that they are imprinted onto the observed warming pattern (shown in Fig. 3a); namely, enhanced Barents and Kara Sea warming, Eastern Pacific cooling, and Southern Ocean cooling (and even cooling in continental Eurasia). Figure S2 shows that the average trend map for i-GWAC (quadrant IV) is essentially the mirror of i-GCAW. While both i-GCAW and i-GWAC patterns have global features agreed upon by over 80% of ensemble members (signified by hatching in Fig. 2), the average i-GWAW and i-GCAC (quadrants I and III) trend maps are focused on the Northern Hemisphere, and do not share consistent global features (see Fig. S2). Note that the trend pattern in Fig. 2 has a mean Arctic warming of 0.126 K/dec and global cooling of -0.021 K/dec, which are roughly 15%

223 weaker than those from the observational estimates in S2023. Using more stringent criterion of
224 global cooling and Arctic warming magnitudes larger than $\frac{3}{4}\boldsymbol{\sigma_{Global}}$ and $\frac{3}{4}\boldsymbol{\sigma_{Arctic}}$ shows similar
225 but stronger features (see Figure S3).

226 The forced SAT trend pattern over 1980-2022 can be obtained from the multi-model
227 mean (MMM) from all large ensembles for the same period. This MMM, however, may have
228 biases due to errors in climate sensitivity and radiative forcings (Tokarska et al., 2020; IPCC
229 chapter 4, 2021). Here we attempt to minimize the impact of these biases by scaling the MMM
230 trend pattern with the observationally estimated forced global trend of 0.213 K/dec for 1980-
231 2022 from S2023. A rough estimate of the global internal trend pattern for 1980-2022 can then
232 be obtained as the difference between observed trends and the scaled MMM trend. Figure 3
233 shows the SAT trend patterns for 1980-2022 from (A) observations, (B) the scaled MMM, and
234 (C) the difference between A and B. While scaling gives us more confidence in the magnitude of
235 the forced trend, it does not change the trend pattern. If the scaled MMM correctly captures the
236 forced pattern of climate change, then the difference in panel C represents the internal trend
237 contribution to the observational record. On the other hand, biases in the simulated forced pattern
238 of warming would produce errors in this estimate of the impact of internal variability.

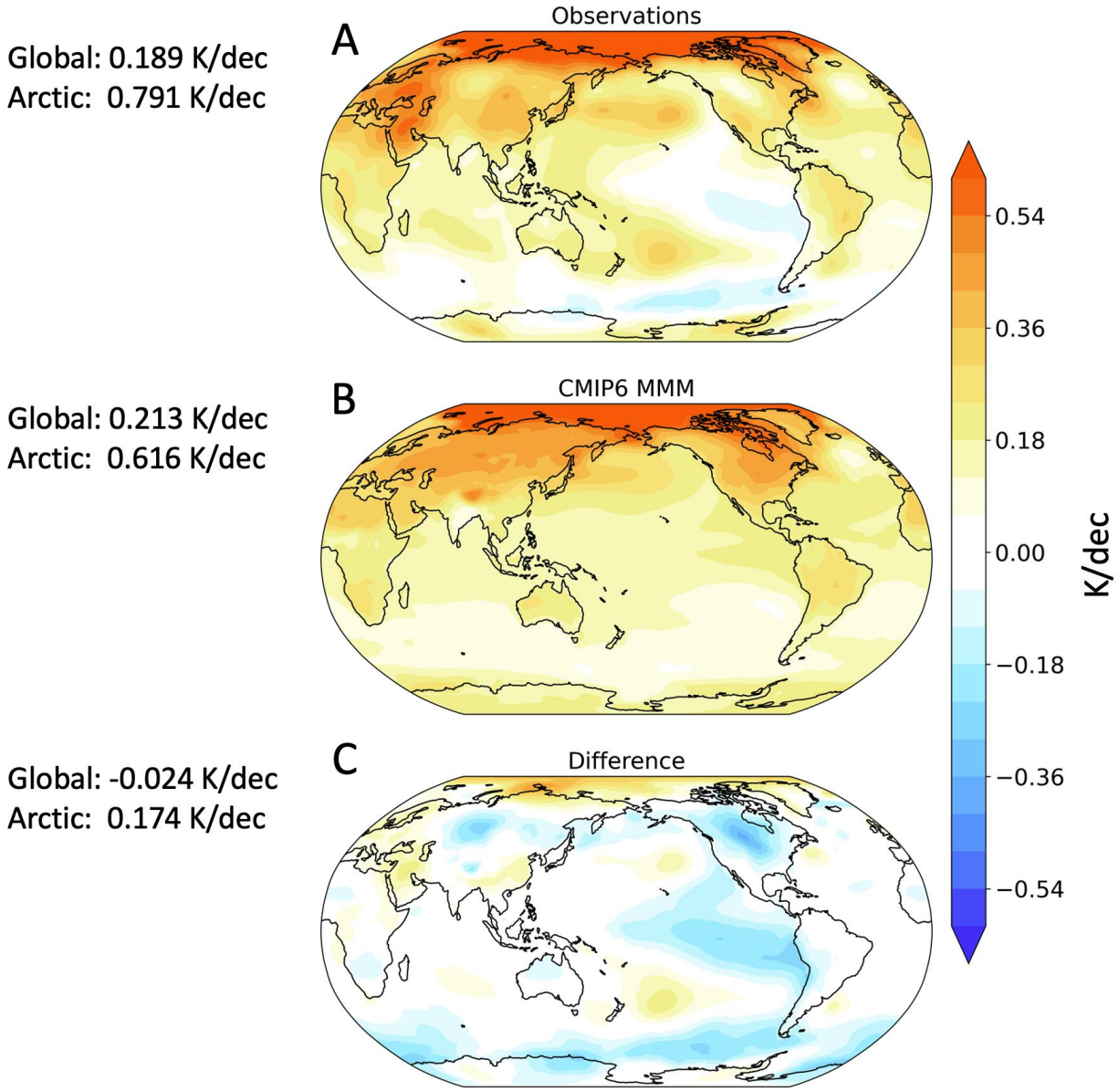

Figure 3: The SAT trend pattern from 1980-2022 in (A) observations, (B) the MMM forced trend scaled by observationally derived global mean forced trend from S2023, and (C) the difference between A and B. Observations are the mean over four observational datasets (see Section 2), and the MMM is the average forced trend from CMIP6 large ensembles scaled so that the global mean warming is equal to 0.213 K/dec (see text).

Observations show many features in the SAT trends not seen in the CMIP6 MMM. While the scaled MMM suggests that external forcing should have produced weak warming throughout the tropical Eastern Pacific and Southern Ocean from 1980-2022, observations exhibit weak cooling in these regions. The difference panel in Fig. 3C shows Arctic warming and cooling in the tropical Eastern Pacific that connects to extensive cooling of the Southern Ocean and is strongest in the Amundsen Sea. Fig. 3C also shows cooling in the northern hemisphere extratropical continents. Notably, many of the features present in the difference pattern of Fig.

3C are also seen in the climate model composite of the internally forced signal shown in Fig. 2. Both figures show warming around the Kara Sea, and cooling throughout the tropical Eastern Pacific and Southern Ocean. The area weighted spatial correlation between the composite trend pattern in Fig. 2 and the difference pattern in Fig. 3C is r=0.49, which may be surprising given that the trend pattern in Fig. 2 is based on model simulated internal variability pre-conditioned only on i-GCAW. The similarity of the global trend patterns from the two methods that are constrained by observations in very different ways strongly suggests that the trend pattern shown in Fig. 3C is significantly impacted by the trend pattern of internal variability in the last few decades if not all caused by the internal variability.

The analysis shown here suggests that from 1980-2022 internal variability manifested as i-GCAW, a rare configuration of internal variability in model simulations. This configuration of internal variability exhibits a unique but robust SAT trend pattern, agreed upon by simulations from different models and over different time periods. Many of the i-GCAW pattern features are also visible in the differences between the observations and the scaled MMM, suggesting that the pattern associated with i-GCAW is imprinted onto the observed SAT trend pattern from 1980-2022. This also suggests that a plausible trend pattern of internal variability can be obtained by solely restricting simulations based on i-GCAW. We next evaluate the implications of this finding and attempt to predict the future evolution of internal variability.

3.2 Implications for Future Arctic Amplification

Fig. 1 suggests that Earth's recent manifestation of internal variability is rare, implying that this configuration cannot persist indefinitely. Fig. 2 showed that this i-GCAW has a robust spatial pattern, with several regions showing strong model agreement. If models also agree on the SAT evolution after the i-GCAW period considered (i.e., 43 years), it may then be possible to predict how this pattern affects future SAT changes. In this section, we attempt to use the simulated i-GCAW cases to predict the future evolution of these patterns and evaluate their implications for AA.

To do this, we take all 136 cases of i-GCAW used to compose Fig. 2 and evaluate the SAT trend evolution over the subsequent 20-years after the i-GCAW was identified. These evolutions of the simulated internal variability are referred to as trajectories and are used to evaluate the potential evolution from the recent observed instance of i-GCAW. Because we only use data from 1850-2047, GCAW patterns that are identified after the 1990-2032 period do not have the full 20-year trajectories available. In these cases, we use the abbreviated trajectory, e.g., if a i-GCAW case is identified over 2000-2042, we just use the trajectory for the following five years. Figure 4A shows the predicted SAT trend patterns after extending the i-GCAW trajectories by 5, 10, 15, and 20 years. Results of Fig. 4A suggest that while cooling trends in the tropical Eastern Pacific degrade after the first decade, the Amundsen Sea cooling trend remains a persistent feature with over 80% of trajectories agreeing on this cooling even when trends are calculated with another 20 years of data. While the trajectories suggest that internally generated Arctic warming will persist in future trend calculations, this signal loses its significance during the second decade of projections. Figure S4 shows a recreation of Fig. 4 using 43-year trends at 5, 10, 15, and 20 years after the initial i-GCAW is identified, (i.e., the 43-year window is shifted by 5, 10, 15, and 20 years to recalculate the role of internal variability). Results of Fig. S4

indicate that the degradation of significance in the Arctic signal shown in Fig. 4 is due to internally driven Arctic trends quickly reverting to near-zero.

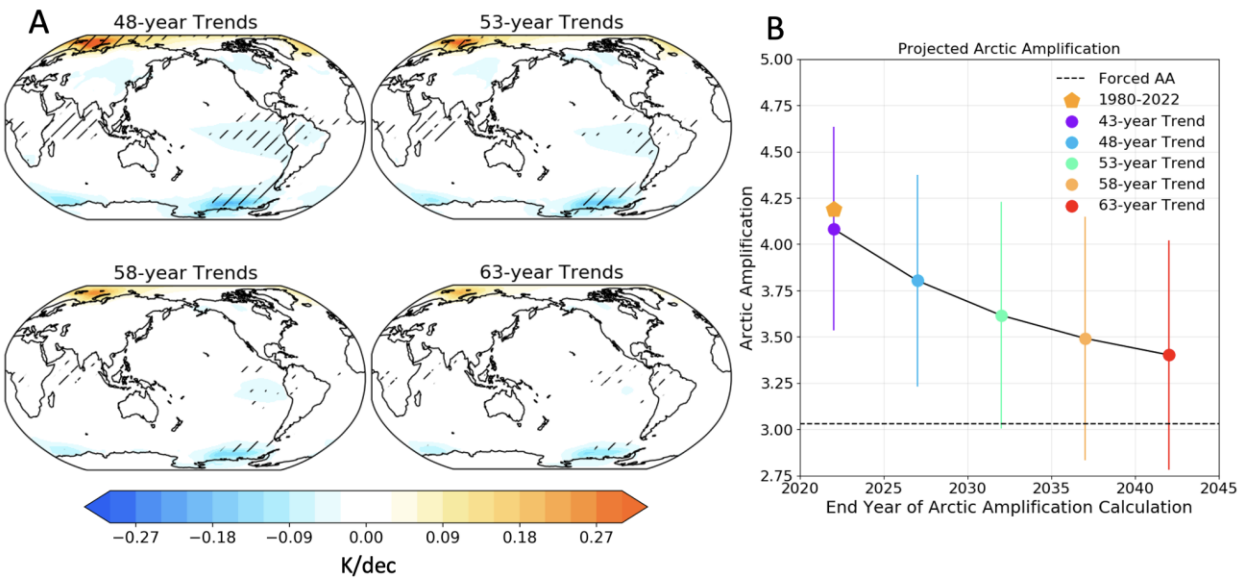

Figure 4: (A) Internally generated SAT trends extended by 5, 10, 15, and 20 years after the i-GCAW pattern has been identified. Hatching indicates regions where over 80% of the cases agree on sign (B) Impact of predicted future configurations of internal variability for Arctic Amplification (AA). Colored dots show model derived AA values given the forced trend (dashed line) from S2023. The orange pentagon shows the AA during the 1980-2022 period from observations. Error bars show the two-sigma confidence interval of future AA using all available trajectories. The black dashed line shows the estimate of the forced AA ratio (3.03) over 1980-2022 from S2023.

Figure 4B shows the future values of AA based on the trajectories of the i-GCAW. The observed AA (shown in orange pentagon) during the 1980-2022 period is inflated above the dashed black line due to internal variability. Based on the mean evolution of the internal trend pattern associated with i-GCAW in Fig. 4A, future values of AA are shown as colored points in Fig 4B. Given that each realization of GCAW in model simulations may have different magnitudes of global-cooling and/or Arctic-warming when identified, all trajectories are computed relative to their initial magnitudes. While on average, the AA metric tends to relax toward the forced trend as the length of time used for the AA calculation increases, the model trajectories indicate that elevated values of AA may persist into the 2040s (England et al., 2015). Fig. 4B suggests that the rare configuration of internal variability that produced large observed values of AA will moderate and AA will subside over the next two decades.

4 Discussion and Conclusions

The observationally inferred trend of internal variability from 1980-2022 suggests global cooling and Arctic warming. Model simulations infrequently simulate this observationally derived variability, suggesting that the Earth experienced a rare configuration of internal variability from 1980 to 2022. To investigate the spatial pattern of SAT trends associated with

the i-GCAW, large ensemble simulations were used to identify cases with the i-GCAW. The spatial SAT trend pattern associated with the i-GCAW is unique, spanning the globe with many robust features, which are distinct from other multi-decadal internal SAT trend patterns (see Fig. S2). These unique and robust features associated with the i-GCAW are also imprinted on the observational record, providing strong evidence that the Earth indeed experienced the i-GCAW from 1980-2022.

Whether discrepancies between climate models and observations are due to a rare configuration of internal variability or model biases in the forced response is a crucial issue in climate science. Of particular importance are the observed cooling trends in the tropical Eastern Pacific over recent decades. These cooling trends generally disagree with simulations which predict a warming response (e.g. Seager et al., 2019). Due to the myriad of teleconnections between this region and higher latitudes (e.g., Trenberth et al., 1998; Baxter et al., 2019), understanding the causes of this discrepancy is important (e.g., Scaife and Smith, 2018; Wanatabe et al., 2021; Wills et al., 2022; Lee et al., 2022). Another area where observations diverge from model predictions is the Southern Ocean. While models predict weak warming (see CMIP6 MMM in Fig. 3), observations show a distinct cooling trend (Kang et al., 2023b). Many plausible drivers have been proposed to explain cooling of the Southern Ocean and its possible connection to the tropical Eastern Pacific, but the relative contribution of different mechanisms is not fully understood (e.g., Latif et al., 2013; Ferreira et al., 2015; Meehl et al., 2016; Hwang et al., 2017; Schneider and Deser, 2017; Zhang et al., 2019; Dong et al., 2022; Hartmann et al., 2022; Dong et al., 2023; Luongo et al., 2023; Roach et al., 2023; Kang et al., 2023a). At the same time, parts of the Arctic have been warming ~7x faster than the global mean over 1980-2022, which may implicate the role of internally driven sea-ice decline associated with atmospheric circulation anomalies (e.g., Ding et al., 2014; England et al., 2019; Day et al., 2012; Svendsen et al., 2021; Isaksen et al., 2022; Roach and Blanchard-Wrigglesworth, 2022). Furthermore, many studies have indicated the potential connection between Arctic warming and Northern Hemisphere continental cooling and the role of internal variability (Cohen et al., 2014; Palmer et al., 2014; Blackport et al., 2019; Fyfe et al., 2019). Our study suggests that the internal variability has made an important contribution together to observed Arctic warming, Eastern Pacific cooling, and Southern Ocean cooling over 1980-2022.

Another notable result of this study is that the model-simulated internal SAT trend pattern associated with the i-GCAW has remarkable similarity to the inferred internal trend pattern by taking the difference between the observed SAT trend and that of the scaled CMIP6 MMM trend (c.f., Fig. 2, and Fig. 3C). These features include many of the aforementioned discrepancies between observations and CMIP6 simulated warming, namely a warming of the Kara Sea concurrent with cooling of the tropical Eastern Pacific and Amundsen Sea, and cooling of parts of central Asia. Importantly, all these features are agreed upon in sign by more than 80% of the simulations considered. This study is consistent with previous research that indicates that internal variability has a strong imprint in these regions individually (e.g., Chen and Dai, 2024; Wanatabe et al., 2021; Zhang et al., 2019) and that internal variability in these regions may even be linked via atmospheric and oceanic teleconnections (Dong et al., 2022; Ding et al., 2014; England et al., 2020). However, it is not necessary that all these features be connected through the same mode of internal variability (Feng et al., 2021). Instead, results here suggest that these internally driven trend patterns are related to the rare manifestation of the i-GCAW, which is responsible for the inflation of AA over recent decades. This also does not preclude the role of

biases in the forced response of models or errors in the historical forcings (Wills et al., 2022; Dong et al., 2022; Tseng et al., 2023; Espinosa et al., 2024), but provides strong evidence that internal variability is a significant contributor to the observed trend pattern.

One noteworthy point is that while the spatial pattern associated with the i-GCAW (Fig. 2) is largely consistent with the difference between observations and the forced response (Fig. 3C), its magnitude is underestimated. This is particularly true in the tropical Eastern Pacific (see comparison of the i-GCAW composite using different thresholds and Fig. 3C in Fig. S3). This discrepancy in the magnitude of the simulated internal variability trend associated with the i-GCAW and the difference pattern may be due to biases in the forced response of climate models (e.g., Seager et al., 2019), biases in the historical forcing exerted to models (e.g., Fasullo et al., 2022), insufficient amplitude of multidecadal internal variability in models (e.g., Laepple et al., 2023), or that other components of internal variability are operating over 1980-2022 that are not captured by the i-GCAW composite.

If part of this discrepancy between Fig. 2 and Fig. 3C (see Fig. S3) in the tropical Eastern Pacific is caused by a bias in the modeled forced response, then this would suggest that the correction of forced response bias has a similar pattern to that of the internal variability in this region. This possibility might complicate efforts to separate forced and unforced climate variability, because many disentanglement techniques are dependent on pattern recognition methodologies (Wills et al. 2020; Po-Chedley et al., 2022). This possibility, however, would not affect our results because a forced response bias with an overestimation of warming in the tropical Eastern Pacific but underestimation of warming in the Arctic at the same time is very unlikely. As previously stated, it is also possible that models do not correctly represent the magnitude of internal variability at multi-decadal timescales (Laepple and Huybers, 2014; Parsons et al., 2017; Kravstov et al., 2018; Feng et al., 2021; Laepple et al., 2023; Stout et al., 2023; Espinosa et al 2024). Similarly, extreme events such as the 2022 heatwave in Antarctica continue to suggest that the observational record is too short in many instances to fully encapsulate the range of internal variability, and that models may not always simulate the full extent of real-world natural variability (Blanchard-Wrigglesworth et al., 2023).

While more research is needed to fully attribute the causes of modeled-versus-observed differences in the pattern of SAT change, the identified pattern of internal variability and its similarity to features in the observational record suggests that the Earth did indeed experience an internally generated global cooling and Arctic warming pattern from 1980-2022. Quantifying the contribution of internal variability to differences in the simulated and observed pattern of SAT change is important because without knowing the relative contribution of internal variability versus biases in the simulated forced response, we are left with significant uncertainties in decadal climate projections (Hu and Deser, 2013; Deser, 2020; Lehner et al., 2020; Wills et al., 2022). This study shows that the internal trend pattern associated with the i-GCAW can account for a significant amount of the discrepancy between observed and CMIP6 simulated patterns of warming from 1980 to 2022. Importantly, this internally generated trend pattern can be obtained by constraining simulations based only on their internally generated global cooling and Arctic warming and calls for further studies focused on this rare manifestation of internal variability.

Acknowledgments

This research was supported by the U.S. Department of Energy (DOE), Office of Science, Office of Biological and Environmental Research, Regional and Global Model Analysis (RGMA) program area, as part of the HiLAT-RASM project. This research was also supported by the NASA FINESST Grant 80NSSC22K1438 and NSF Grant AGS-2202812. Additional funding was provided by the Calvin Professorship in Atmospheric Sciences. S.P.-C was supported through the PCMDI Project, which is funded by the RGMA program area of the Office of Science at DOE. M. Wang is funded with support of the Arctic Research Program of the NOAA Global Ocean Monitoring and Observing (GOMO) office through the Cooperative Institute for Climate, Ocean, & Ecosystem Studies (CICOES) under NOAA Cooperative Agreement NA20OAR4320271, Contribution No 2024-yyyy, and Pacific Marine Environmental Laboratory Contribution No zzzz. Research at Lawrence Livermore National Laboratory was performed under the auspices of U.S. DOE Contract DE-AC52-07NA27344. The Pacific Northwest National Laboratory (PNNL) is operated for DOE by Battelle Memorial Institute under contract DE-AC05-76RLO1830. We would like to acknowledge high-performance computing support from Cheyenne (doi:10.5065/D6RX99HX) provided by NCAR's Computational and Information Systems Laboratory, sponsored by the National Science Foundation, for the analyses presented in this study and for data management, storage, and preservation.

Open Research

The data on which this article is based is the same as was used in S2023 and be found at https://zenodo.org/records/8286633.

References

Barnes, E. A., Hurrell, J. W., Ebert-Uphoff, I., Anderson, C., & Anderson, D. (2019). Viewing Forced Climate Patterns Through an AI Lens. *Geophysical Research Letters*, *46*(22), 13389–13398. https://doi.org/10.1029/2019GL084944

Baxter, I., Ding, Q., Schweiger, A., L'Heureux, M., Baxter, S., Wang, T., et al. (2019). How Tropical Pacific Surface Cooling Contributed to Accelerated Sea Ice Melt from 2007 to 2012 as Ice Is Thinned by Anthropogenic Forcing. *Journal of Climate*, *32*(24), 8583–8602. https://doi.org/10.1175/JCLI-D-18-0783.1

Blackport, R., Screen, J. A., van der Wiel, K., & Bintanja, R. (2019). Minimal influence of reduced Arctic sea ice on coincident cold winters in mid-latitudes. *Nature Climate Change*, *9*(9), 697–704. https://doi.org/10.1038/s41558-019-0551-4

441 Blanchard-Wrigglesworth, E., Cox, T., Espinosa, Z. I., & Donohoe, A. (2023). The Largest Ever
442 Recorded Heatwave—Characteristics and Attribution of the Antarctic Heatwave of March
443 2022. *Geophysical Research Letters*, *50*(17), e2023GL104910.
444 https://doi.org/10.1029/2023GL104910
445 Chylek, P., Folland, C., Klett, J. D., Wang, M., Hengartner, N., Lesins, G., & Dubey, M. K.
446 (2022). Annual Mean Arctic Amplification 1970–2020: Observed and Simulated by CMIP6
447 Climate Models. *Geophysical Research Letters*, *49*(13), e2022GL099371.
448 https://doi.org/10.1029/2022GL099371
449 Chylek, P., Folland, C. K., Klett, J. D., Wang, M., Lesins, G., & Dubey, M. K. (2023). High
450 Values of the Arctic Amplification in the Early Decades of the 21st Century: Causes of
451 Discrepancy by CMIP6 Models Between Observation and Simulation. *Journal of*
452 *Geophysical Research: Atmospheres*, *128*(23), e2023JD039269.
453 https://doi.org/10.1029/2023JD039269
454 Cohen, J., Screen, J. A., Furtado, J. C., Barlow, M., Whittleston, D., Coumou, D., et al. (2014).
455 Recent Arctic amplification and extreme mid-latitude weather. *Nature Geoscience*, *7*(9),
456 627–637. https://doi.org/10.1038/ngeo2234
457 Dai, A., Fyfe, J. C., Xie, S.-P., & Dai, X. (2015). Decadal modulation of global surface
458 temperature by internal climate variability. *Nature Climate Change*, *5*(6), 555–559.
459 https://doi.org/10.1038/nclimate2605
460 Day, J. J., Hargreaves, J. C., Annan, J. D., & Abe-Ouchi, A. (2012). Sources of multi-decadal
461 variability in Arctic sea ice extent. *Environmental Research Letters*, *7*(3), 034011.
462 https://doi.org/10.1088/1748-9326/7/3/034011

463 Deser, C. (2020). "Certain Uncertainty: The Role of Internal Climate Variability in Projections
464 of Regional Climate Change and Risk Management." *Earth's Future*, *8*(12),
465 e2020EF001854. https://doi.org/10.1029/2020EF001854
466 Deser, C., Knutti, R., Solomon, S., & Phillips, A. S. (2012). Communication of the role of
467 natural variability in future North American climate. *Nature Climate Change*, *2*(11), 775–
468 779. https://doi.org/10.1038/nclimate1562
469 Deser, C., Phillips, A., Bourdette, V., & Teng, H. (2012). Uncertainty in climate change
470 projections: the role of internal variability. *Climate Dynamics*, *38*(3), 527–546.
471 https://doi.org/10.1007/s00382-010-0977-x
472 Deser, C., Phillips, A. S., Alexander, M. A., & Smoliak, B. V. (2014). Projecting North
473 American Climate over the Next 50 Years: Uncertainty due to Internal Variability. *Journal*
474 *of Climate*, *27*(6), 2271–2296. https://doi.org/10.1175/JCLI-D-13-00451.1
475 Deser, C., Phillips, A. S., Simpson, I. R., Rosenbloom, N., Coleman, D., Lehner, F., et al. (2020).
476 Isolating the Evolving Contributions of Anthropogenic Aerosols and Greenhouse Gases: A
477 New CESM1 Large Ensemble Community Resource. *Journal of Climate*, *33*(18), 7835–
478 7858. https://doi.org/10.1175/JCLI-D-20-0123.1
479 Ding, Q., & Steig, E. J. (2013). Temperature Change on the Antarctic Peninsula Linked to the
480 Tropical Pacific. *Journal of Climate*, *26*(19), 7570–7585. https://doi.org/10.1175/JCLI-D-
481 12-00729.1
482 Ding, Q., Wallace, J. M., Battisti, D. S., Steig, E. J., Gallant, A. J. E., Kim, H.-J., & Geng, L.
483 (2014). Tropical forcing of the recent rapid Arctic warming in northeastern Canada and
484 Greenland. *Nature*, *509*(7499), 209–212. https://doi.org/10.1038/nature13260

Ding, Q., Schweiger, A., L'Heureux, M., Steig, E. J., Battisti, D. S., Johnson, N. C., et al. (2019). Fingerprints of internal drivers of Arctic sea ice loss in observations and model simulations. *Nature Geoscience*, *12*(1), 28–33. https://doi.org/10.1038/s41561-018-0256-8

Dong, Y., Pauling, A. G., Sadai, S., & Armour, K. C. (2022). Antarctic Ice-Sheet Meltwater Reduces Transient Warming and Climate Sensitivity Through the Sea-Surface Temperature Pattern Effect. *Geophysical Research Letters*, *49*(24), e2022GL101249. https://doi.org/10.1029/2022GL101249

England, M., Jahn, A., & Polvani, L. (2019). Nonuniform Contribution of Internal Variability to Recent Arctic Sea Ice Loss. *Journal of Climate*, *32*(13), 4039–4053. https://doi.org/10.1175/JCLI-D-18-0864.1

England, M. H., Kajtar, J. B., & Maher, N. (2015). Robust warming projections despite the recent hiatus. *Nature Climate Change*, *5*(5), 394–396. https://doi.org/10.1038/nclimate2575

England, M. R., Polvani, L. M., & Sun, L. (2020). Robust Arctic warming caused by projected Antarctic sea ice loss. *Environmental Research Letters*, *15*(10), 104005. https://doi.org/10.1088/1748-9326/abaada

Fasullo, J. T., Lamarque, J.-F., Hannay, C., Rosenbloom, N., Tilmes, S., DeRepentigny, P., et al. (2022). Spurious Late Historical-Era Warming in CESM2 Driven by Prescribed Biomass Burning Emissions. *Geophysical Research Letters*, *49*(2), e2021GL097420. https://doi.org/10.1029/2021GL097420

Feng, X., Ding, Q., Wu, L., Jones, C., Baxter, I., Tardif, R., et al. (2021). A Multidecadal-Scale Tropically Driven Global Teleconnection over the Past Millennium and Its Recent Strengthening. *Journal of Climate*, *34*(7), 2549–2565. https://doi.org/10.1175/JCLI-D-20-0216.1

508 Ferreira, D., Marshall, J., Bitz, C. M., Solomon, S., & Plumb, A. (2015). Antarctic Ocean and
509 Sea Ice Response to Ozone Depletion: A Two-Time-Scale Problem. *Journal of Climate*,
510 *28*(3), 1206–1226. https://doi.org/10.1175/JCLI-D-14-00313.1
511 Foster, G., & Rahmstorf, S. (2011). Global temperature evolution 1979–2010. *Environmental*
512 *Research Letters*, *6*(4), 044022. https://doi.org/10.1088/1748-9326/6/4/044022
513 Fyfe, J. C. (2019). Midlatitudes unaffected by sea ice loss. *Nature Climate Change*, *9*(9), 649–
514 650. https://doi.org/10.1038/s41558-019-0560-3
515 Gordon, E. M., Barnes, E. A., & Hurrell, J. W. (2021). Oceanic Harbingers of Pacific Decadal
516 Oscillation Predictability in CESM2 Detected by Neural Networks. *Geophysical Research*
517 *Letters*, *48*(21), e2021GL095392. https://doi.org/10.1029/2021GL095392
518 Hahn, L. C., Armour, K. C., Zelinka, M. D., Bitz, C. M., & Donohoe, A. (2021). Contributions to
519 Polar Amplification in CMIP5 and CMIP6 Models. *Frontiers in Earth Science*, *9*. Retrieved
520 from https://www.frontiersin.org/articles/10.3389/feart.2021.710036
521 Hansen, J., Ruedy, R., Sato, M., & Lo, K. (2010). Global Surface Temperature Change. *Reviews*
522 *of Geophysics*, *48*(4). https://doi.org/10.1029/2010RG000345
523 Hartmann, D. L. (2022). The Antarctic ozone hole and the pattern effect on climate sensitivity.
524 *Proceedings of the National Academy of Sciences*, *119*(35), e2207889119.
525 https://doi.org/10.1073/pnas.2207889119
526 Hu, A., & Deser, C. (2013). Uncertainty in future regional sea level rise due to internal climate
527 variability. *Geophysical Research Letters*, *40*(11), 2768–2772.
528 https://doi.org/10.1002/grl.50531

Hwang, Y.-T., Xie, S.-P., Deser, C., & Kang, S. M. (2017). Connecting tropical climate change with Southern Ocean heat uptake. *Geophysical Research Letters*, *44*(18), 9449–9457. https://doi.org/10.1002/2017GL074972

Intergovernmental Panel on Climate Change (IPCC) (Ed.). (2023). Future Global Climate: Scenario-based Projections and Near-term Information. In *Climate Change 2021 – The Physical Science Basis: Working Group I Contribution to the Sixth Assessment Report of the Intergovernmental Panel on Climate Change* (pp. 553–672). Cambridge: Cambridge University Press. https://doi.org/10.1017/9781009157896.006

Isaksen, K., Nordli, Ø., Ivanov, B., Køltzow, M. A. Ø., Aaboe, S., Gjelten, H. M., et al. (2022). Exceptional warming over the Barents area. *Scientific Reports*, *12*(1), 9371. https://doi.org/10.1038/s41598-022-13568-5

Kang, S. M., Shin, Y., Kim, H., Xie, S.-P., & Hu, S. (2023). Disentangling the mechanisms of equatorial Pacific climate change. *Science Advances*, *9*(19), eadf5059. https://doi.org/10.1126/sciadv.adf5059

Kang, S. M., Yu, Y., Deser, C., Zhang, X., Kang, I.-S., Lee, S.-S., et al. (2023). Global impacts of recent Southern Ocean cooling. *Proceedings of the National Academy of Sciences*, *120*(30), e2300881120. https://doi.org/10.1073/pnas.2300881120

Kay, J. E., Deser, C., Phillips, A., Mai, A., Hannay, C., Strand, G., et al. (2015). The Community Earth System Model (CESM) Large Ensemble Project: A Community Resource for Studying Climate Change in the Presence of Internal Climate Variability. *Bulletin of the American Meteorological Society*, *96*(8), 1333–1349. https://doi.org/10.1175/BAMS-D-13-00255.1

Kay, Jennifer E., Holland, M. M., & Jahn, A. (2011). Inter-annual to multi-decadal Arctic sea ice extent trends in a warming world. *Geophysical Research Letters*, *38*(15). https://doi.org/10.1029/2011GL048008

Kosaka, Y., & Xie, S.-P. (2013). Recent global-warming hiatus tied to equatorial Pacific surface cooling. *Nature*, *501*(7467), 403–407. https://doi.org/10.1038/nature12534

Kravtsov, S., Grimm, C., & Gu, S. (2018). Global-scale multidecadal variability missing in state-of-the-art climate models. *Npj Climate and Atmospheric Science*, *1*(1), 1–10. https://doi.org/10.1038/s41612-018-0044-6

Labe, Z. M., & Barnes, E. A. (2022). Predicting Slowdowns in Decadal Climate Warming Trends With Explainable Neural Networks. *Geophysical Research Letters*, *49*(9), e2022GL098173. https://doi.org/10.1029/2022GL098173

Laepple, T., & Huybers, P. (2014). Global and regional variability in marine surface temperatures. *Geophysical Research Letters*, *41*(7), 2528–2534. https://doi.org/10.1002/2014GL059345

Laepple, T., Ziegler, E., Weitzel, N., Hébert, R., Ellerhoff, B., Schoch, P., et al. (2023). Regional but not global temperature variability underestimated by climate models at supradecadal timescales. *Nature Geoscience*, *16*(11), 958–966. https://doi.org/10.1038/s41561-023-01299-9

Latif, M., Martin, T., & Park, W. (2013). Southern Ocean Sector Centennial Climate Variability and Recent Decadal Trends. *Journal of Climate*, *26*(19), 7767–7782. https://doi.org/10.1175/JCLI-D-12-00281.1

Lee, S., L'Heureux, M., Wittenberg, A. T., Seager, R., O'Gorman, P. A., & Johnson, N. C. (2022). On the future zonal contrasts of equatorial Pacific climate: Perspectives from

574 Observations, Simulations, and Theories. *Npj Climate and Atmospheric Science*, *5*(1), 1–15.
575 https://doi.org/10.1038/s41612-022-00301-2
576 Lehner, F., & Deser, C. (2023). Origin, importance, and predictive limits of internal climate
577 variability. *Environmental Research: Climate*, *2*(2), 023001. https://doi.org/10.1088/2752-
578 5295/accf30
579 Lehner, F., Deser, C., Maher, N., Marotzke, J., Fischer, E. M., Brunner, L., et al. (2020).
580 Partitioning climate projection uncertainty with multiple large ensembles and CMIP5/6.
581 *Earth System Dynamics*, *11*(2), 491–508. https://doi.org/10.5194/esd-11-491-2020
582 Lenssen, N. J. L., Schmidt, G. A., Hansen, J. E., Menne, M. J., Persin, A., Ruedy, R., & Zyss, D.
583 (2019). Improvements in the GISTEMP Uncertainty Model. *Journal of Geophysical*
584 *Research: Atmospheres*, *124*(12), 6307–6326. https://doi.org/10.1029/2018JD029522
585 Manabe, S., & Wetherald, R. T. (1975). The Effects of Doubling the CO2 Concentration on the
586 climate of a General Circulation Model. *Journal of the Atmospheric Sciences*, *32*(1), 3–15.
587 https://doi.org/10.1175/1520-0469(1975)032<0003:TEODTC>2.0.CO;2
588 Meehl, G. A., Arblaster, J. M., Bitz, C. M., Chung, C. T. Y., & Teng, H. (2016). Antarctic sea-
589 ice expansion between 2000 and 2014 driven by tropical Pacific decadal climate variability.
590 *Nature Geoscience*, *9*(8), 590–595. https://doi.org/10.1038/ngeo2751
591 Morice, C. P., Kennedy, J. J., Rayner, N. A., Winn, J. P., Hogan, E., Killick, R. E., et al. (2021).
592 An Updated Assessment of Near-Surface Temperature Change From 1850: The HadCRUT5
593 Data Set. *Journal of Geophysical Research: Atmospheres*, *126*(3), e2019JD032361.
594 https://doi.org/10.1029/2019JD032361
595 Palmer, T. (2014). Record-breaking winters and global climate change. *Science*, *344*(6186), 803–
596 804. https://doi.org/10.1126/science.1255147

Parsons, L. A., Loope, G. R., Overpeck, J. T., Ault, T. R., Stouffer, R., & Cole, J. E. (2017). Temperature and Precipitation Variance in CMIP5 Simulations and Paleoclimate Records of the Last Millennium. *Journal of Climate*, *30*(22), 8885–8912. https://doi.org/10.1175/JCLI-D-16-0863.1

Po-Chedley, S., Fasullo, J. T., Siler, N., Labe, Z. M., Barnes, E. A., Bonfils, C. J. W., & Santer, B. D. (2022). Internal variability and forcing influence model–satellite differences in the rate of tropical tropospheric warming. *Proceedings of the National Academy of Sciences*, *119*(47), e2209431119. https://doi.org/10.1073/pnas.2209431119

Rader, J. K., Barnes, E. A., Ebert-Uphoff, I., & Anderson, C. (2022). Detection of Forced Change Within Combined Climate Fields Using Explainable Neural Networks. *Journal of Advances in Modeling Earth Systems*, *14*(7), e2021MS002941. https://doi.org/10.1029/2021MS002941

Räisänen, J. (2021). Effect of atmospheric circulation on surface air temperature trends in years 1979–2018. *Climate Dynamics*, *56*(7), 2303–2320. https://doi.org/10.1007/s00382-020-05590-y

Rantanen, M., Karpechko, A. Y., Lipponen, A., Nordling, K., Hyvärinen, O., Ruosteenoja, K., et al. (2022). The Arctic has warmed nearly four times faster than the globe since 1979. *Communications Earth & Environment*, *3*(1), 1–10. https://doi.org/10.1038/s43247-022-00498-3

Roach, L. A., & Blanchard-Wrigglesworth, E. (2022). Observed Winds Crucial for September Arctic Sea Ice Loss. *Geophysical Research Letters*, *49*(6), e2022GL097884. https://doi.org/10.1029/2022GL097884

619 Roach, Lettie A., Mankoff, K. D., Romanou, A., Blanchard-Wrigglesworth, E., Haine, T. W. N.,
620 & Schmidt, Gavin. A. (2023). Winds and Meltwater Together Lead to Southern Ocean
621 Surface Cooling and Sea Ice Expansion. *Geophysical Research Letters*, *50*(24),
622 e2023GL105948. https://doi.org/10.1029/2023GL105948
623 Rohde, R. A., & Hausfather, Z. (2020). The Berkeley Earth Land/Ocean Temperature Record.
624 *Earth System Science Data*, *12*(4), 3469–3479. https://doi.org/10.5194/essd-12-3469-2020
625 Rosenblum, E., & Eisenman, I. (2017). Sea Ice Trends in Climate Models Only Accurate in Runs
626 with Biased Global Warming. *Journal of Climate*, *30*(16), 6265–6278.
627 https://doi.org/10.1175/JCLI-D-16-0455.1
628 Scaife, A. A., & Smith, D. (2018). A signal-to-noise paradox in climate science. *Npj Climate and*
629 *Atmospheric Science*, *1*(1), 1–8. https://doi.org/10.1038/s41612-018-0038-4
630 Schlesinger, M. E., & Ramankutty, N. (1994). An oscillation in the global climate system of
631 period 65–70 years. *Nature*, *367*(6465), 723–726. https://doi.org/10.1038/367723a0
632 Schneider, D. P., & Deser, C. (2018). Tropically driven and externally forced patterns of
633 Antarctic sea ice change: reconciling observed and modeled trends. *Climate Dynamics*,
634 *50*(11), 4599–4618. https://doi.org/10.1007/s00382-017-3893-5
635 Screen, J. A., & Deser, C. (2019). Pacific Ocean Variability Influences the Time of Emergence
636 of a Seasonally Ice-Free Arctic Ocean. *Geophysical Research Letters*, *46*(4), 2222–2231.
637 https://doi.org/10.1029/2018GL081393
638 Seager, R., Cane, M., Henderson, N., Lee, D.-E., Abernathey, R., & Zhang, H. (2019).
639 Strengthening tropical Pacific zonal sea surface temperature gradient consistent with rising
640 greenhouse gases. *Nature Climate Change*, *9*(7), 517–522. https://doi.org/10.1038/s41558-
641 019-0505-x

642 Stout, R. C., Proistosescu, C., & Roe, G. (2023). Fingerprinting Low-Frequency Last Millennium
643 Temperature Variability in Forced and Unforced Climate Models. *Journal of Climate*,
644 *36*(20), 7005–7023. https://doi.org/10.1175/JCLI-D-22-0810.1
645 Stuecker, M. F., Bitz, C. M., & Armour, K. C. (2017). Conditions leading to the unprecedented
646 low Antarctic sea ice extent during the 2016 austral spring season. *Geophysical Research*
647 *Letters*, *44*(17), 9008–9019. https://doi.org/10.1002/2017GL074691
648 Svendsen, L., Keenlyside, N., Muilwijk, M., Bethke, I., Omrani, N.-E., & Gao, Y. (2021).
649 Pacific contribution to decadal surface temperature trends in the Arctic during the twentieth
650 century. *Climate Dynamics*, *57*(11), 3223–3243. https://doi.org/10.1007/s00382-021-05868-
651 9
652 Sweeney, A. J., Fu, Q., Po-Chedley, S., Wang, H., & Wang, M. (2023). Internal Variability
653 Increased Arctic Amplification During 1980–2022. *Geophysical Research Letters*, *50*(24),
654 e2023GL106060. https://doi.org/10.1029/2023GL106060
655 Tokarska, K. B., Stolpe, M. B., Sippel, S., Fischer, E. M., Smith, C. J., Lehner, F., & Knutti, R.
656 (2020). Past warming trend constrains future warming in CMIP6 models. *Science Advances*,
657 *6*(12), eaaz9549. https://doi.org/10.1126/sciadv.aaz9549
658 Trenberth, K. E., Branstator, G. W., Karoly, D., Kumar, A., Lau, N.-C., & Ropelewski, C.
659 (1998). Progress during TOGA in understanding and modeling global teleconnections
660 associated with tropical sea surface temperatures. *Journal of Geophysical Research:*
661 *Oceans*, *103*(C7), 14291–14324. https://doi.org/10.1029/97JC01444
662 Tseng, H.-Y., Hwang, Y.-T., Xie, S.-P., Tseng, Y.-H., Kang, S. M., Luongo, M. T., & Eisenman,
663 I. (2023). Fast and Slow Responses of the Tropical Pacific to Radiative Forcing in Northern

High Latitudes. *Journal of Climate*, *36*(16), 5337–5349. https://doi.org/10.1175/JCLI-D-22-0622.1

Watanabe, M., Dufresne, J.-L., Kosaka, Y., Mauritsen, T., & Tatebe, H. (2021). Enhanced warming constrained by past trends in equatorial Pacific sea surface temperature gradient. *Nature Climate Change*, *11*(1), 33–37. https://doi.org/10.1038/s41558-020-00933-3

Wills, R. C. J., Battisti, D. S., Armour, K. C., Schneider, T., & Deser, C. (2020). Pattern Recognition Methods to Separate Forced Responses from Internal Variability in Climate Model Ensembles and Observations. *Journal of Climate*, *33*(20), 8693–8719. https://doi.org/10.1175/JCLI-D-19-0855.1

Wills, R. C. J., Dong, Y., Proistosecu, C., Armour, K. C., & Battisti, D. S. (2022). Systematic Climate Model Biases in the Large-Scale Patterns of Recent Sea-Surface Temperature and Sea-Level Pressure Change. *Geophysical Research Letters*, *49*(17), e2022GL100011. https://doi.org/10.1029/2022GL100011

Xie, S.-P. (2020). Ocean Warming Pattern Effect On Global And Regional Climate Change. *AGU Advances*, *1*(1), e2019AV000130. https://doi.org/10.1029/2019AV000130

Xie, S.-P., & Kosaka, Y. (2017). What Caused the Global Surface Warming Hiatus of 1998–2013? *Current Climate Change Reports*, *3*(2), 128–140. https://doi.org/10.1007/s40641-017-0063-0

Ye, K., & Messori, G. (2021). Inter-model spread in the wintertime Arctic amplification in the CMIP6 models and the important role of internal climate variability. *Global and Planetary Change*, *204*, 103543. https://doi.org/10.1016/j.gloplacha.2021.103543

Zhang, J. H. L., B. Huang, M. J. Menne, X. Yin, A. Sánchez-Lugo, B. E. Gleason, Russell Vose, D. Arndt, J. J. Rennie, C. N. (2019, July 19). Updated Temperature Data Give a Sharper

687 View of Climate Trends. Retrieved May 30, 2023, from http://eos.org/science-
688 updates/updated-temperature-data-give-a-sharper-view-of-climate-trends
689 Zhang, L., Delworth, T. L., Cooke, W., & Yang, X. (2019). Natural variability of Southern
690 Ocean convection as a driver of observed climate trends. *Nature Climate Change*, *9*(1), 59–
691 65. https://doi.org/10.1038/s41558-018-0350-3
692